Journal of Ceramic Processing Research. Vol. 24, No. 1, pp. 197~204 (2023)
(Received 21 September 2022, Received in revised form 17 December 2022, Accepted 3 January 2023)
https://doi.org/10.36410/jcpr.2023.24.1.197

J O U R N A L O F
Ceramic Processing Research

The effect of ceramic fiber on the rheological and mechanical properties of porous Al_2O_3 ceramics

Kamrun Nahar Fatema[a], Hyung Mi Lim[b], Joung Sook Hong[c], Kee Sung Lee[d] and Ik Jin Kim[a,*]
[a]*Institute of Processing and Application of Inorganic Materials (PAIM), Department of Materials Science and Engineering, Hanseo University, Chungcheongnam-do 31962, Korea*
[b]*Korea Institute of Ceramic Engineering & Technology (KICET), Jinju 52851, Korea*
[c]*School of Chemical and Biological Engineering, Institute of Chemical Processes, Seoul National University, Seoul 08826, Korea*
[d]*School of Mechanical Engineering, Kookmin University, Seoul 02707, Korea*

Porous ceramics having oriented pores find widespread use in filtration, insulation, biomaterials, and catalysis. Because of the shape of the interconnected pores, porous alumina (Al_2O_3) ceramics synthesized via direct foaming have poor mechanical strength. The physical and mechanical characteristics of porous Al_2O_3 ceramics were systematically explored in this work by modulating the microstructure and rheological properties by the inclusion of ceramic fibers. Because of the incorporation of ceramic fibers, the fiber-containing wall structure is generated in porous ceramics. The physical properties and mechanical strength of porous ceramics increase as the fiber content increases. To stabilize the wet foam and enhance the mechanical properties of the porous ceramics, ceramic fibers are added to the Al_2O_3 colloidal suspension. With 2.0 wt.% ceramic fibers, wet foam stability of 84% was obtained. Adequate addition of 2.0 wt.% ceramic fibers in the slurry may improve compressive strength, however excess fibers reduce compressive strength. The load-bearing capacity and elastic modulus of sintered samples were determined using the Hertzian indentation method. The load-bearing capacity and elastic modulus increased from 65.35 to 235.45 N and 28.52 to 270.75 MPa, respectively, as the ceramic fiber content increased from 0.5 to 3.0 wt.%.

Keywords: Colloidal suspension, Ceramic fiber, Direct foaming, Porous ceramics, Hertzian method.

Introduction

In the areas of filtration, insulation, biomaterials, separation media for molten metals, hot gases, and catalysis, porous ceramics with oriented pores have several uses due to their low density, high specific surface area, good corrosion and wear resistance [1, 2]. Al_2O_3 ceramics offer outstanding physical and chemical qualities, including high strength, hardness, insulating resistance, and corrosion resistance. These ceramics also benefit from plentiful raw material sources, cheap cost, and reasonably developed processing and production capabilities [3]. The performance of ceramic composites is determined by the ceramic characteristics, volume percentages, bonding qualities, phase interface and bonding strength [4].

Porous ceramics strength depends on porosity, pore shape, ceramic wall width, and ceramic bridges between neighboring walls. Slurry particles determine porous ceramic porosity. Solid content increases porosity linearly. Porosity decreases mechanical properties of porous materials [4]. Understanding the effect of porosity, shape, size, and pore distribution is critical for producing highly effective porous ceramics for a variety of applications [5]. Porous ceramics are thought to provide suitable components for the development of advanced composites with high chemical and thermal stability requirements because they have high stiffness, thermal stability, and a comparatively low density.To increase the mechanical strength of porous ceramics, various fibers such as carbon fiber [6], glass fiber [7], and ceramic fiber [8] have been introduced. Porous ceramics may be processed in three ways: replica methods [9], sacrificial template [10], and direct foaming also, direct foaming is especially well adapted to the modification of open and closed pore structures with porosities ranging from 45 to 85% and cell diameters ranging from 30 μm to 1 mm [11, 12].

Porous ceramics are produced via direct foaming methods by mechanically frothing air bubbles into a colloidal suspension. When the suspension sets, the cavities generated by the air bubbles in the structure form pores. In this case, the moulded and dried foams are sintered at high temperatures thereafter to produce porous ceramics. Directly foamed ceramics have a total porosity that is proportional to the number of air

*Corresponding author:
Tel : +82-41-660-1441
Fax: +82-41-660-1441
E-mail: ijkim@hanseo.ac.kr, keeslee@kookmin.ac.kr

bubbles added into the colloidal suspension during the foaming process [13]. Because of pores, pore distribution, and surface defects, it is difficult to quantify the mechanical strength of highly porous ceramics using a conventional bending test.

The wet foam stability of a particle-stabilized colloidal suspension after foaming was explored in this work, as well as the enhancement of mechanical properties of porous ceramics by the addition of ceramic fiber. To make a colloidal suspension, we used Al_2O_3 powder and polygallate as particles and amphiphiles, respectively, for foam stabilization.

Hardness is a property value that reflects a material's resistance to surface deformation or abrasion. Additionally, it correlates with mechanical qualities like as tensile strength. We evaluated the elastic modulus and compressive load of porous samples, which has the advantage of characterizing the load-bearing capacity with local fracture using hard-sphere and elastic modulus by analyzing the mechanical behavior of loading or unloading curves rather than compressive strength measurements [14, 15]. Using conventional tests of strength, such porous ceramics are utterly brittle. Increased ceramic fiber content formed an interconnected neck-foam in Al_2O_3 porous ceramics, which enhanced their mechanical properties [16-18]. We obtained reliable multiple data for each sample using a tungsten carbide (WC) sphere in the Hertzian indentation method [19], whereas the conventional method for testing compressive strengths could obtain only a single data per sample.

This study provides how direct foaming improved the mechanical characteristics of Al_2O_3 porous ceramics made from particle-stabilized colloidal suspension with the addition of ceramic fiber. In terms of wet foam stability and the physical characteristics of porous ceramics, the effect of ceramic fiber on air content, bubble size, pore size, and pore distribution was studied.

Experimental Procedure

Raw materials and preparation of colloidal suspension

Powdered α-Al_2O_3 (KC, South Korea) with an average diameter d_{50} of 0.4 μm was used as the starting material to prepare the initial colloidal suspension. Ceramic fiber (Mitsubishi Chemical) was used to improve the wet foam stability and mechanical properties of the suspension (Fig. 1). The primary phases of the ceramic fibers include Al_2O_3 and silicon dioxide (SiO_2), as revealed by energy-dispersive X-ray (EDX) analysis. The diameter and length of the ceramic fiber were approximately 5 μm and 0.1-0.3 μm, respectively. Propyl gallate (Fluka Analytical, Germany) was used for the surface modification of Al_2O_3 particles. Furthermore, to modulate the pH of the colloidal suspension to pH 4.5, hydrochloric acid (Yakuri Pure Chemicals; Osaka, Japan) and deionized water were used to prepare the final suspension. The colloidal suspension of α-Al_2O_3 to wet foam containing ceramic fibers was conducted by mechanical frothing following the procedure reported in [20]. They directly incorporated air bubbles into a colloidal suspension by hand mixing to create pores. Porous ceramics were obtained after drying and sintering.

Rheological Property measurements

The rheological properties of the Al_2O_3 suspension containing ceramic fibers were measured using a rotational rheometer (MCR502, Anton Paar, Germany) with the cone-cup type configuration (CC27) at room temperature. The dynamic oscillation mode was chosen to study the linear viscoelasticity (LVE) of the slurry. The viscoelasticity of the slurry was determined by the storage modulus (G′) and loss modulus (G″) analysis. The storage modulus represents the elastic contribution of viscoelastic behavior, whereas the loss modulus characterizes the viscous contribution of the viscoelastic behavior of a slurry. An oscillatory strain amplitude sweep test was conducted to determine the range of linear viscoelastic strain for the slurry at room temperature. G′ and G″ were measured at strain amplitude sweep from 10^{-3} to 10 [-] at a fixed angular frequency of 1 rad/s. A steady-flow test was conducted at the shear rate of 1-1000 s^{-1} to check the shear dependency, yielding behavior, and limit of the linear viscoelastic range of the slurry [21].

Colloidal suspension and wet foam

Due to the large, highly energetic interfacial area, the bubbles coarsen in a process involving drainage, coalescence, and Ostwald ripening. The thermodynamic instability of the wet foam bubbles in the colloidal suspension is the main challenge in processing such foams. The pressure acting on gas bubbles in a liquid can be described by the Laplace pressure as follows:

$$\Delta P = \gamma\left(\frac{1}{R_1}+\frac{1}{R_2}\right) = \frac{2\gamma}{R} \text{ (for spherical bubbles)} \qquad (1)$$

where ΔP is the Laplace pressure, R_1 and R_2 are the principal radii of curvature and γ is the surface tension. To avoid foam collapse in the wet state, the air-liquid interface of the foams must be stabilized. Typically, the surface tension of the gas-liquid interface is reduced using surfactants or proteins to reduce the Laplace pressure and prolong the lifespan of the newly formed bubbles. The Gibbs free energy for particle detachment from the air-water interface describes how well particles with different sizes and contact angles are adsorbed to the air-water interface. It is expressed as the energy needed to remove a particle from the interface into the bulk water. The adsorption free energy (ΔG) can be expressed as follows:

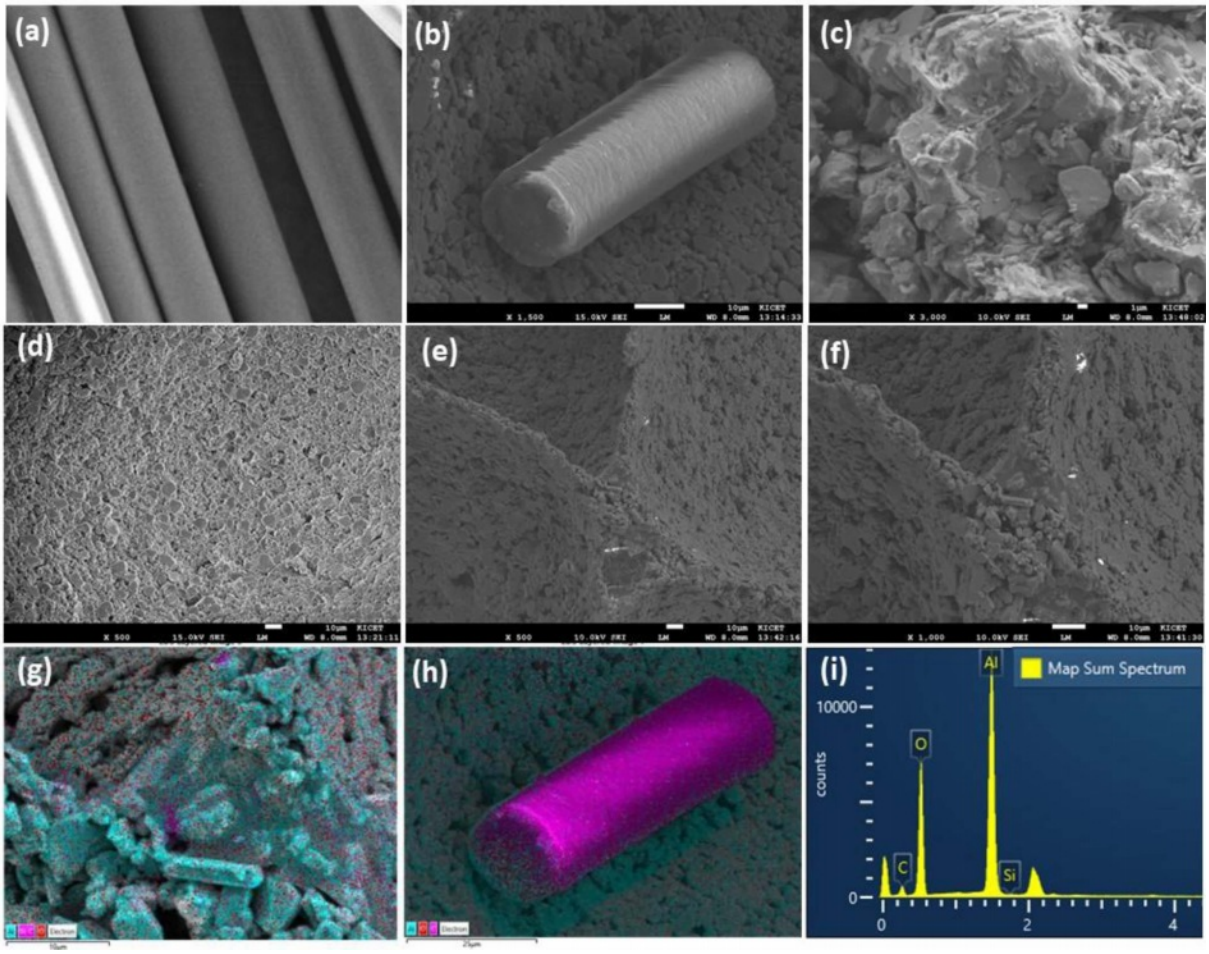

Fig. 1. (a) Field-emission scanning electron microscope (FESEM) image of ceramic fiber, (b) layered image, (c) microstructure, (d) electron image, (e-f) pore wall, (g-h) eds layered image of ceramic fiber reinforced Al_2O_3 and (i) energy dispersion X-ray (EDX) spectra.

$$\Delta G = \pi r^2 \gamma_{\alpha\beta}(1-\cos\theta)^2 \text{ for } \theta \leq 90^o \quad (2)$$

where r is the radius of the adsorbed particles θ, $\gamma_{\alpha\beta}$ is the surface tension, and θ is the contact angle [18]. Herein, bubble and pore sizes were measured using an optical microscope after dropping a wet foam formed by direct foaming from the colloidal suspension on a glass plate. The air content and wet foam stability were calculated using the equation reported in [20].

Mechanical properties

The wet samples were dried enough at room

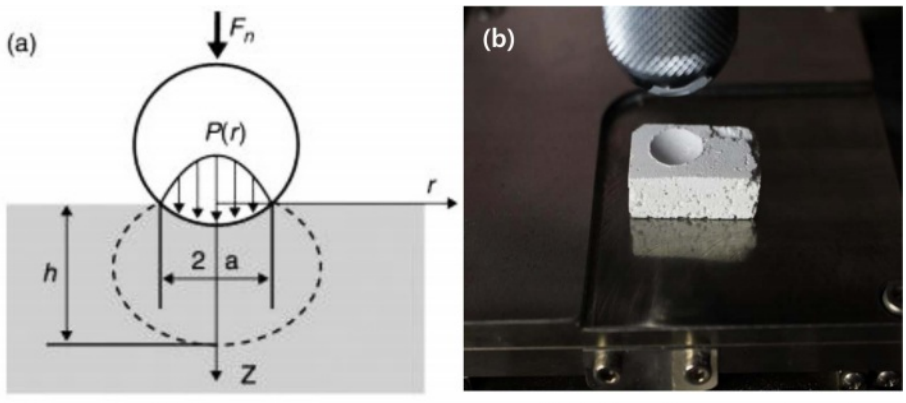

a) Hertz pressure b) Indentation experiment

Fig. 2. (a) Schematic of the Hertzian pressure distribution during indentation. (b) Indentation on 0.5 wt.% ceramic-fiber-reinforced porous Al_2O_3 ceramics using a WC sphere.

temperature for 48 h and heat-treated at 1,500 °C for 1 h in an Argon environment to sinter the body. The heating and cooling rates were maintained at 1 and 3 °C/min, respectively. The samples were machined to bar specimens of dimensions 25 mm × 25 mm × 12 mm, and the surface was polished with SiC abrasive paper (#1,200) to evaluate the mechanical properties of the porous ceramics by Hertzian indentation, as shown in Fig. 2.

Hertzian indentation was performed on the surface of porous ceramics using a WC sphere (J&L Industry, USA) of radius r = 7.93 mm with loads of up to 200 N using a universal testing machine (Model 5567, Instron Corporation, Canton, MA) in air. A schematic of the pressure distribution using hard sphere is shown in Fig. 2(a). The same crosshead speed at 0.2 mm/min was applied during the loading and unloading of the WC sphere in the experiment. The indentation load-displacement curves were plotted during loading, and the loading was stopped when the depth displacement reached h = 2 mm (Fig. 2(b)). The elastic modulus of the sample was calculated from slopes of the loading curve, and the maximum load value was recorded.

Results and Discussion

According to Eq. (3), for the colloidal suspension and wet foam characterizations, wet foam stability of 65% from particle-stabilized colloidal suspension to porous Al_2O_3 ceramics was obtained at a particle contact angle of 60.87° with a surface tension of 18.31 mN/m.

$$\text{Wet foam stability} = \frac{V_{Final}}{V_{Initial}} \times 100\% \quad (3)$$

The combined effect of the particle attachment energy of 3.1×10^{-12} J and Laplace pressure of 0.98 N/mm results in the wet foam stability of 84% with 2.0 wt.% of ceramic fiber.

Fig. 1(a) shows the FESEM images of the ceramic fiber. Fig. 1(b-d) depicts the layered image, microstructure, and electron image of ceramic fiber reinforced Al_2O_3, revealing a significant change in the morphology of the samples. Fig. 1(e-f) depicts the cross-sectional morphology that indicated that the inclusion of ceramic fiber increased grain coarsening of pore wall. Although it is not a distinguishable differentiation, it has had a significant impact on mechanical strength. Fig. 1(g-h) displays the EDS layered image and Energy dispersive spectroscopy (EDS) was utilized to qualitatively examine the chemical composition of ceramic fiber reinforced Al_2O_3 shown in Fig. 1(i).

Fig. 3 shows the results of the strain-amplitude sweep test of the suspensions with different fiber contents. The test was conducted at strain ranging from 10^{-3} to 10 and fixed angular frequency of 1 rad/s to measure G′ and G″ of the slurry. The strain range

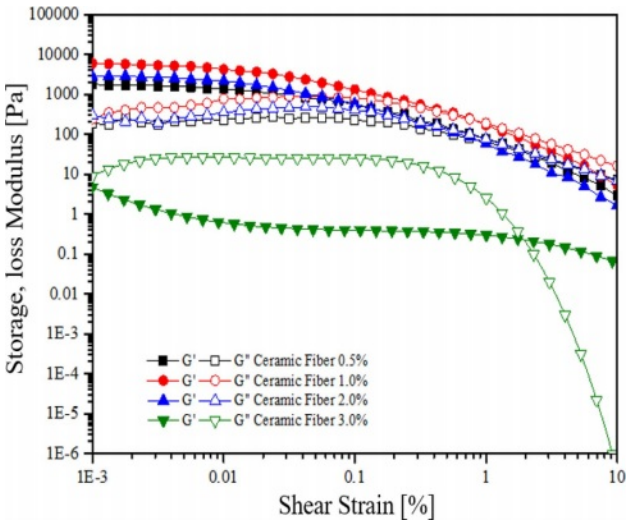

Fig. 3. Storage and loss moduli of Al_2O_3 suspension as functions of ceramic fiber content.

where G′ and G″ remain almost constant is the LVE region, and the limiting value of the LVE region is the critical point where the slurry starts to deform nonlinearly. Then, the slurry responds differently to a large nonlinear strain range, depending on its structure. The suspension showed a limited LVE behaviour at a low-strain range. When compared to our prior published work [27] for Al_2O_3 suspension and with a small amount of fiber, less than 2 wt.%, G′ was higher than G″ until the strain reached 0.2-0.4. Then, G″ became higher than G′, indicating that the suspension started to flow, and the particles or particle aggregates moved along with the deformation. Meanwhile, the suspension with 3.0 wt.% fiber showed a decreased modulus, and its G′ was constant, whereas G″ changed significantly over the observation range. G′ was higher than G″ as the strain increased above 2.0. Al_2O_3 particles in the suspension showed weak interactions, and the particle dispersion structure was easily changed under small strain, even with a ceramic fiber content of less than 2.0 wt.%. With the ceramic fiber content above 2.0 wt.%, particles in the suspensions were tightly bound together. They aligned along the flow as the shear strain increased [21]. The presence of ceramic fiber less than 2.0 wt.% did not significantly affect the flow behaviour of the suspension. However, with ceramic fiber contents above 2.0 wt.%, the interaction among Al_2O_3 particles in the suspension was influenced by the presence of ceramic fibers. The interaction between the ceramic fiber and Al_2O_3 particles more dynamically compete under strain to build up a flow-induced dispersion structure of hybrid particles.

Fig. 4 shows the viscosity of the Al_2O_3 colloidal suspension with ceramic fiber. The viscosity of the Al_2O_3 slurry decreased with an increase in shear rate, resulting in a shear-thinning behavior. However, as the amount of ceramic fiber increased, the viscosity gradually

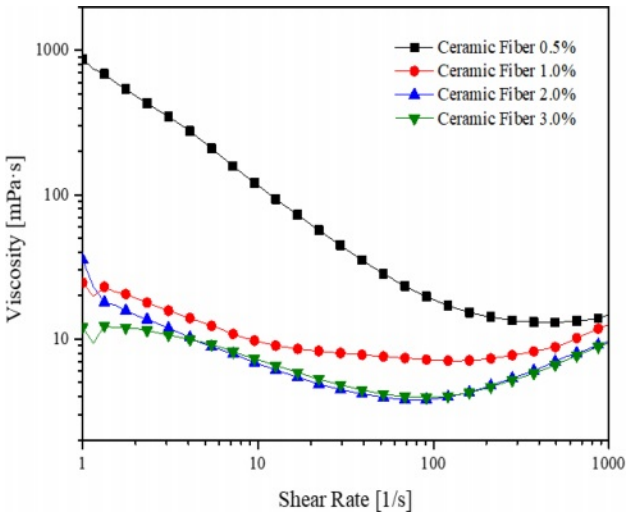

Fig. 4. Viscosity of Al_2O_3 suspensions as a function of ceramic fiber content.

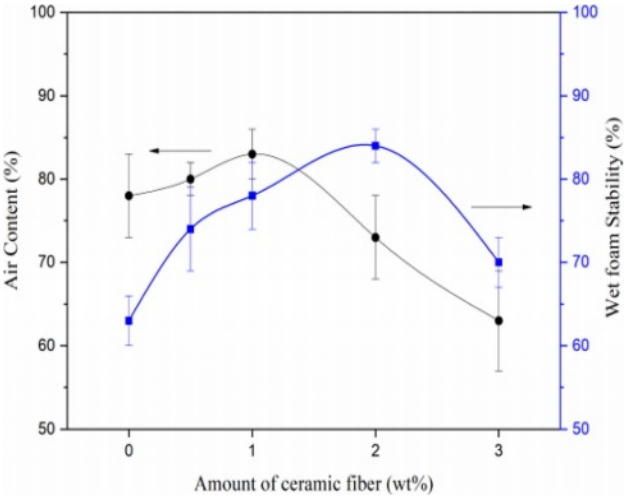

Fig. 5. Air content and wet foam stability of Al_2O_3 suspensions as functions of ceramic fiber content.

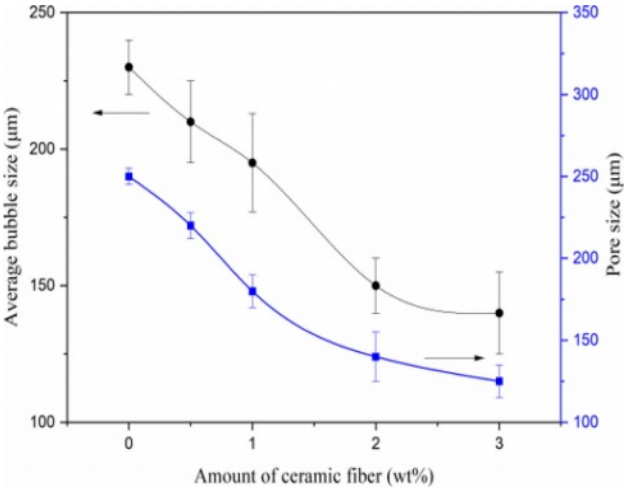

Fig. 6. Average bubble and pore size of Al_2O_3 suspensions as functions of ceramic fiber content.

decreased compared to Al_2O_3 suspension which is published our previous work [27], shear-thinning behavior disappeared, and the shear dependency of viscosity became insignificant. As the ceramic fiber content increased from 0.5 to 3.0 wt.%, the viscosity of the suspension remarkably decreased, and the shear dependency of viscosity changed.

This implies that the addition of ceramic fiber to Al_2O_3 suspension significantly affects the dispersion of Al_2O_3 particles. The dispersion of propyl-gallate-treated Al_2O_3 particles is disrupted by the presence of ceramic fibers. The hydrophobic interaction among particles bound by the van der Waals force may be disturbed by the ionic interaction among fibers, resulting in the heterogeneous dispersion structure of hybrid particles and remarkable change in the rheological behavior [22]. Herein, the suspensions with a mixture of Al_2O_3 and ceramic fiber slowly developed shear-thinning-thickening behavior as the shear rate increased only when the fiber content increased above 2.0 wt.%, indicating that as shear rate increases, the hybrid particles generate different particle dispersion structures. The shear-thickening behavior of the suspension possibly provides more uniform air bubble generation during the foaming process [23] as it restricts air bubble growth, resulting in homogeneous small foam generation, even at high shear rates.

Fig. 5 shows the relationship between the air content and wet foam stability from Al_2O_3 particle-stabilized colloidal suspension as a function of ceramic fiber content. A high-capacity foam was obtained with an air content of up to 83% foamed by mechanical frothing with maximum wet foam stability of 78%, indicating the stabilization of the wet foam due to the adhesion of particles at the air–water interface. The wet foam stability and air content are shown in Fig. 5. As the ceramic fiber content increased from 0.5 to 1.0 wt.%, the air content and wet foam stability increased. As the ceramic fiber content was further increased from 2.0 to 3.0 wt.%, the air content maintained its values, and the wet foam stability decreased from 84% to 70%.

Fig. 6 shows the relationship between the average bubble and pore sizes as functions of the ceramic fiber content. The colloidal suspension without ceramic fiber had pore sizes of 230 μm created from air content of 63% with a bubble size of 230 μm. The pore size was 150-230 μm and uniformly distributed (Fig. 7a). The bubble and pore sizes decreased as the ceramic fiber content increased to 3.0 wt.%, This is because the pressure difference at the air-water interface collapsed the bubbles in the wet foam. As a result, the range of pore size was controlled from 140 to 230 μm in this study.

Fig. 7 shows the microstructures of porous Al_2O_3 ceramics sintered at 1500 °C for 1 h as a function of ceramic fiber content. The microstructures were

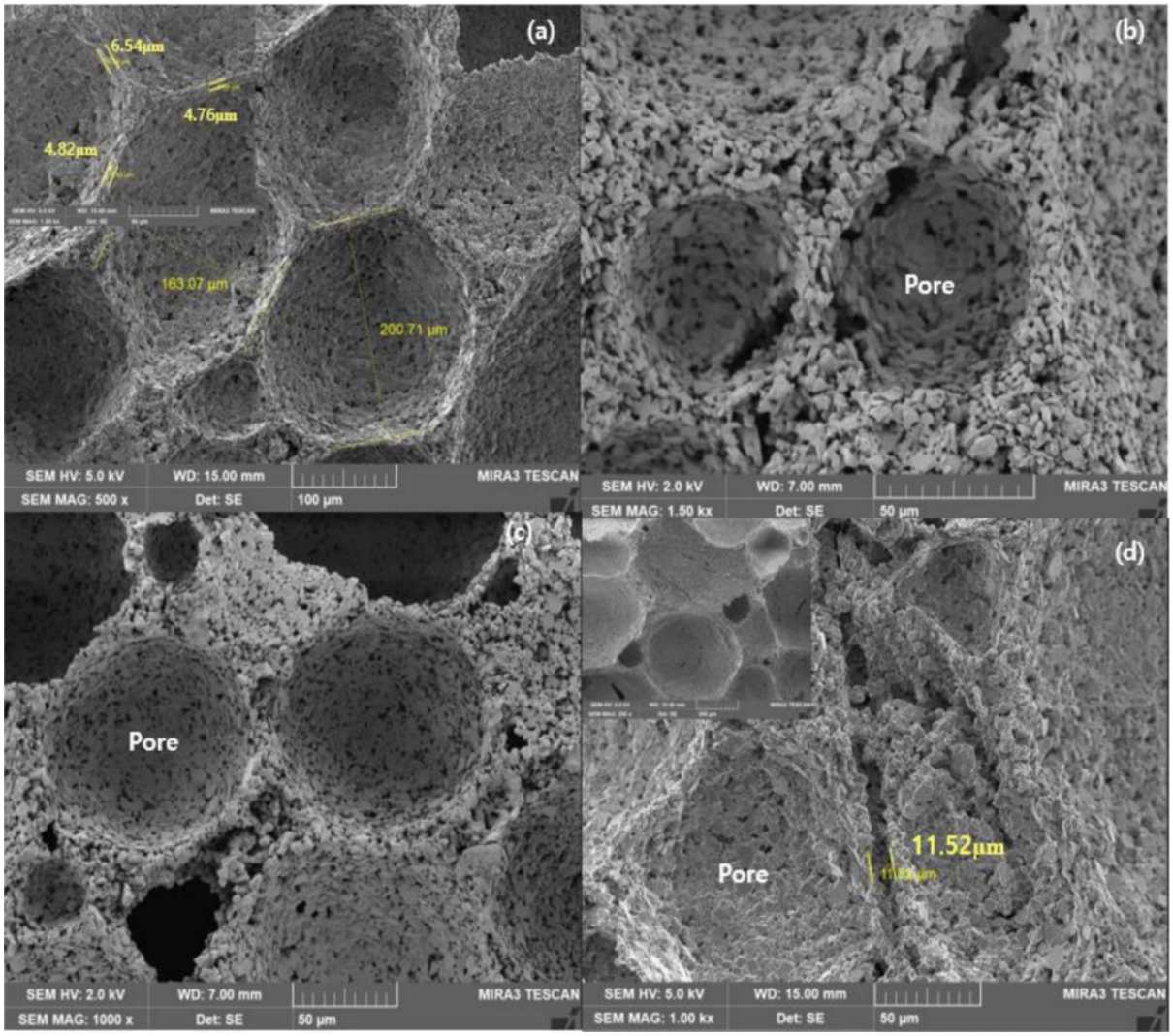

Fig. 7. Field emission scanning electron microscopy (FESEM) images of the porous Al_2O_3 ceramics sintered at 1500 °C for 1 h with ceramic fiber content of (a) 0 wt.%, (b) 0.5 wt.%, (c) 1.0 wt.%, and (d) 3.0 wt.%.

composed of closed and interconnected pores with a relatively uniform size distribution. The thickness of the porous Al_2O_3 ceramic film was 4.76-6.54 μm, and the pore size (163.07-200.71 μm) was uniformly distributed. Although the ceramic fibers disappeared during the firing process, those between pore walls overcame the destabilization mechanisms, including Ostwald ripening, which is a result of the diffusion of small bubbles into large bubbles [24]. Fig. 5 and Table 1 show that when up to 2.0 wt.% ceramic fibers was added to the colloidal suspension, the wet foam became more stable, and the mechanical properties of the porous ceramics were improved.

Fig. 8 shows the indentation load-displacement curves of porous Al_2O_3 ceramics with different ceramic fiber contents (0, 0.5, 1, 2, and 3 wt.%). The curves were obtained by indenting with a WC sphere with a radius r = 7.93 mm until the sphere reached a maximum of 2 mm depth. The porous Al_2O_3 ceramics without ceramic fiber exhibited considerably lower load-bearing

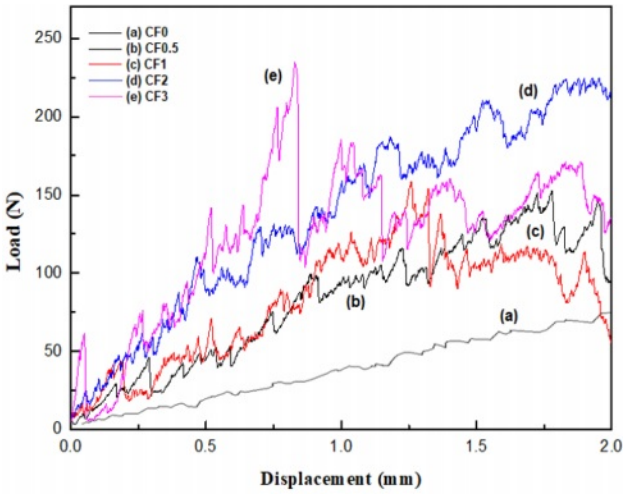

Fig. 8. Compressive load-displacement curve for porous Al_2O_3 ceramics sintered at 1500 °C for 1 h with ceramic fiber content of (a) 0 wt.%, (b) 0.5 wt.%, (c) 1.0 wt.%, (d) 2.0 wt.%, and (e) 3.0 wt.%.

Table 1. Physical and mechanical properties of porous Al_2O_3 ceramics.

Sample	Density [g/cm^3]	Pore size [μm]	Porosity [%]	Elastic modulus [MPa]	Compressive load [N]
Al_2O_3-CF0	0.270	230	58.35	28.52	65.35
Al_2O_3-CF0.5	0.443	210	54.27	110.53	158.45
Al_2O_3-CF1	0.469	195	56.37	120.56	162.35
Al_2O_3-CF2	0.475	150	62.24	175.23	225.23
Al_2O_3-CF3	0.426	140	64.70	270.75	235.45

capacity than those with high ceramic fiber contents. Quasi-plastic behavior [25] was observed, even in the high-elastic Al_2O_3 ceramics, indicating a high porosity effect (Fig. 7). On the other hand, porous Al_2O_3 ceramics with 3.0 wt.% ceramic fiber exhibited high load-bearing capacity, thus could endure a maximum compressive load of 235.45 N at the same displacement. Notably, it has a relatively small pore size of about 140 μm (Table 1). As the ceramic fiber content increased to 3.0 wt.%, the pore size became smaller and more uniform; thus, the load-bearing capacity increased. The slope of the mechanical behavior curve also increased as the ceramic fiber content increased to 3.0 wt.%, indicating that the addition of ceramic fiber improved the elastic modulus of the porous sample.

Table 1 lists the physical and mechanical properties of porous Al_2O_3 ceramics with different ceramic fiber contents as a foaming agent. The ceramic fiber improved most physical and mechanical properties of the ceramics. The mechanical properties, such as elastic modulus and compressive load, showed the maximum value with the highest porosity. The density of the porous Al_2O_3 ceramics without ceramic fiber, which was the lowest (0.270 g/cm^3), was increased to 0.426 g/cm^3 by adding 3.0 wt.% ceramic fiber. The pore size and porosity of Al_2O_3 without ceramic fiber were relatively high, and the porous Al_2O_3 ceramics with 3.0 wt.% of ceramic fiber exhibited a pore size of 140 μm with porosity of 64.70%. Due to the very high porosity of the Al_2O_3-CF3 sample, which comes in at 64.70 percent, the samples density is much lower than that of other Al_2O_3-CF samples. In addition to that, the sample has a rather high elastic modulus as well as a tensile strength [26, 27]. As the ceramic fiber content increased to 3.0 wt.%, the maximum load and elastic modulus increased from 65.35 to 235.45 N and 28.52 to 270.75 MPa, respectively.

Conclusions

In this study, we investigated the effect of ceramic fiber content on the wet foam stability and rheological properties of colloidal Al_2O_3 suspensions and the improvement on the mechanical properties of the porous Al_2O_3 ceramics. With 2.0 wt.% ceramic fiber, the suspension showed wet foam stability of 84% and air content of 73%. The cell size of the wet foam was at least 250 μm without ceramic fibers and decreased to 135 μm with the addition of 3.0 wt.% ceramic fiber. The ceramic fibers in the pore films maintain the stability of the bubble sizes, increasing the wet foam stability. After sintering, the porosity of the ceramic increased with the ceramic fiber content. Analysis using the Hertzian method revealed that the addition of ceramic fibers improved the mechanical properties of porous Al_2O_3 ceramics. The elastic modulus increased from 28.522 to 270.75 MPa, and the maximum load-bearing capacity increased from 65.35 to 235.45 N as the ceramic fiber increased to 3.0 wt.%.

Acknowledgements

This study was supported by Hanseo University.

References

1. N. Zhang, Z. Liu, Y. Du, Q. Yu, S. Wang, G. Tan, B. Jiang, Z. Zhang, and R.O. Ritchie, J. Eur. Ceram. Soc. 42[15] (2022) 7196-7202.
2. H. Qiu, H. Sun, X. Liu, H. Sui, and D. Huang, J. Mater. Sci.: Mater. Electron. 33[15] (2022) 12171-12181.
3. J. Hu, Q. Huang, H. Peng, X. Tian, Z. Chen, and Y. Peng, J. Ceram. Process. Res. 19[3] (2018) 224-230.
4. J.-G. Song, Y. Liu, C.L. Pang, J. Zhang, L. Chen, X. Zhang, S. Guo, X. Wang, R. Wang, and A. Chen, J. Ceram. Process. Res. 19[2] (2018) 142-145.
5. S. Meille, M. Lombardi, J. Chevalier, and L. Montanaro, J. Eur. Ceram. Soc. 32[15] (2012) 3959-3967.
6. S. Mazumder, J.G. Park, N. Sakar, K.S. Lee, B. Basnet, and I.J. Kim, J. Ceram. Process. Res. 17[12] (2016) 1274-1278.
7. F.-W. Zok and C.G. Levi, Adv. Eng. Mater. 3[1,2] (2001) 15-23.
8. B.-H. Kim and Y.H. Na, Ceram. Int. 21[6] (1995) 381-384.
9. Y.-W. Kim, Y.J. Jin, Y.S. Chun, I.H. Song, and H.D. Kim, Scr. Mater. 53[8] (2005) 921-925.
10. K. Araki and J.W. Halloran, J. Am. Ceram. Soc. 87[10] (2004) 1859-1863.
11. W.-Y. Jang, D.N. Seo, B. Basnet, J.G. Park, I.S. Han, and I.J. Kim, J. Ceram. Process. Res. 18[4] (2017) 275-279.
12. Z. Chu, C. Jia, J. Liu, R. Ding, and A. Zhang, J. Ceram. Process. Res. 18[2] (2017) 127-126.
13. B.-S.M. Seeber, U.T. Gonenbach, and L. Gauckler, J. Mater. Res. 28[17] (2013) 2281-2286.
14. K.-H. Lee and K.W. Nam, J. Ceram. Process. Res. 19[1] (2018) 75-79.

15. S.-H. Ahn and K.W. Nam, J. Ceram. Process. Res. 18[9] (2017) 646-658.
16. H.-W. Cheong, S.H. Ha, and Y.S. Choi, J. Ceram. Process. Res. 13[2] (2012) 308-311.
17. J. Hu, X. Tian, C. Hu, Y. Luo, H. Peng, and J. Luo, J. Ceram. Process. Res. 17[11] (2016) 1181-1187.
18. J.-G. Song, Y. Liu, C.L. Pang, J. Zhang, L. Chen, X. Zhang, S. Guo, X. Wang, R. Wang, and A. Chen, J. Ceram. Process. Res. 19[2] (2018) 142-145.
19. B. Basnet, H.M. Lim, K.S. Lee, and I.J. Kim, J. Korean Ceram. Soc. 56[5] (2019) 513-520.
20. N. Sarkar, K.S. Lee, J.G. Park, S. Mazumder, I.S. Han, and I.J. Kim, Ceram. Int. 42[2] (2016) 3548-3555.
21. C. Voigt, C.G. Aneziris, and J. Hubalkova, J. Am. Ceram. Soc. 98[5] (2015) 1460-1463.
22. N. Sarkar, J.G. Park, S. Bhaskar, S. Mazumder, D.N. Seo, and I. J. Kim, Ceram. Int. 41[3] (2015) 4021-4027.
23. X. Dong, X. Xu, and Z. Liu, Chem. Eng. Res. Des. 168[1] (2021) 288-296.
24. A.-R. Studart, U.T. Gonzenbach, E. Tervoort, and L.J. Gauckler, J. Am. Ceram. Soc. 89[6] (2006) 1771-1789.
25. B.-R. Lawn, J. Am. Ceram. Soc. 81[8] (1998) 1977-1994.
26. L. Pupure, J. Varna, R. Joffe, F. Berthold, and A. Miettinen, Wood Mater. Sci. Eng. 15[2] (2020) 76-86.
27. B. Basnet, H.M. Lim, K.S. Lee, and I.J. Kim, Journal of the Korean Ceramic Society 56[5] (2019) 513-520.